Monthly Notices
of the
ROYAL ASTRONOMICAL SOCIETY

MNRAS **464,** 2419–2428 (2017)
Advance Access publication 2016 September 28

doi:10.1093/mnras/stw2461

The low-mass end of the baryonic Tully–Fisher relation

Laura V. Sales,[1⋆] Julio F. Navarro,[2†] Kyle Oman,[2] Azadeh Fattahi,[2] Ismael Ferrero,[3,4] Mario Abadi,[3,4] Richard Bower,[5] Robert A. Crain,[6] Carlos S. Frenk,[5] Till Sawala,[7] Matthieu Schaller,[5] Joop Schaye,[8] Tom Theuns[5] and Simon D. M White[9]

[1]*Department of Physics and Astronomy, University of California, Riverside, CA, 92521, USA*
[2]*Department of Physics and Astronomy, University of Victoria, Victoria, BC V8P 5C2, Canada*
[3]*Observatorio Astronómico, Universidad Nacional de Córdoba, Córdoba, X5000BGR, Argentina*
[4]*Instituto de Astronomía Teórica y Experimental – CONICET, Laprida 922 X5000BGR, Argentina*
[5]*Department of Physics, Institute for Computational Cosmology, University of Durham, South Road, Durham DH1 3LE, UK*
[6]*Astrophysics Research Institute, Liverpool John Moores University, 146 Brownlow Hill, Liverpool L3 5RF, UK*
[7]*Department of Physics, University of Helsinki, Gustaf Hällströmin katu 2a, FI-00014 Helsinki, Finland*
[8]*Leiden Observatory, Leiden University, PO Box 9513, NL-2300 RA Leiden, the Netherlands*
[9]*Max Planck Institute for Astrophysics, D-85748 Garching, Germany*

Accepted 2016 September 27. Received 2016 September 23; in original form 2016 February 3

ABSTRACT

The scaling of disc galaxy rotation velocity with baryonic mass (the 'baryonic Tully–Fisher' relation, BTF) has long confounded galaxy formation models. It is steeper than the $M \propto V^3$ scaling relating halo virial masses and circular velocities and its zero-point implies that galaxies comprise a very small fraction of available baryons. Such low galaxy formation efficiencies may, in principle, be explained by winds driven by evolving stars, but the tightness of the BTF relation argues against the substantial scatter expected from such a vigorous feedback mechanism. We use the APOSTLE/EAGLE simulations to show that the BTF relation is well reproduced in Λcold dark matter (CDM) simulations that match the size and number of galaxies as a function of stellar mass. In such models, galaxy rotation velocities are proportional to halo virial velocity and the steep velocity-mass dependence results from the decline in galaxy formation efficiency with decreasing halo mass needed to reconcile the CDM halo mass function with the galaxy luminosity function. The scatter in the simulated BTF is smaller than observed, even when considering all simulated galaxies and not just rotationally supported ones. The simulations predict that the BTF should become increasingly steep at the faint end, although the velocity scatter at fixed mass should remain small. Observed galaxies with rotation speeds below ∼40 km s^{-1} seem to deviate from this prediction. We discuss observational biases and modelling uncertainties that may help to explain this disagreement in the context of ΛCDM models of dwarf galaxy formation.

Key words: galaxies: evolution – galaxies: haloes – galaxies: structure.

1 INTRODUCTION

The empirical relation between the rotation velocity and luminosity of disc galaxies is not only a reliable secondary distance indicator (Tully & Fisher 1977), but also provides important clues to the total mass and mass profiles of their host dark matter haloes. The Tully–Fisher (TF) relation has now been extensively studied observationally; its dependence on photometric passband, in particular, is relatively well understood, and the relation is now generally cast in terms of galaxy stellar mass rather than luminosity (e.g. McGaugh et al. 2000; Bell & de Jong 2001; Pizagno et al. 2005; Torres-Flores et al. 2011).

This relation is well approximated by a single power law with small scatter, at least for late-type galaxies with stellar masses $\gtrsim 10^{9.5}$ M$_\odot$ and velocities $\gtrsim$65 km s^{-1} (McGaugh et al. 2000; Bell & de Jong 2001). At lower masses/velocities, the relation deviates from a simple power law, presumably because the contribution of cold gas becomes more and more prevalent in dwarf galaxies. Indeed, the power-law scaling may be largely rectified at the faint end by considering baryonic masses rather than stellar mass alone. The 'baryonic Tully–Fisher' relation, as this relation has become known (or BTF, for short), is well approximated by a single power

⋆ E-mail: lsales@ucr.edu
† Senior CIfAR Fellow.

law over roughly three decades in mass and a factor of 6 in velocity (McGaugh et al. 2000; Verheijen 2001; Stark, McGaugh & Swaters 2009). Its scatter is quite small, at least when only galaxies with high-quality data and radially extended rotation curves are retained for analysis (McGaugh 2012; Lelli, McGaugh & Schombert 2016).

The interpretation of the TF relation in cosmologically motivated models of galaxy formation has long been problematic. From a cosmological viewpoint, the TF relation is understood as reflecting the equivalence between halo mass and circular velocity imposed by the finite age of the Universe (see, e.g. Mo, Mao & White 1998; Steinmetz & Navarro 1999). That characteristic time-scale translates into a fixed density contrast that implies a linear scaling between virial[1] radius and velocity, or a simple $M \propto V^3$ relation between mass and circular velocity. A power-law scaling between galaxy mass and disc rotation velocity is therefore expected if galaxy mass and rotation speed scale with virial mass and virial velocity, respectively.

The latter conditions are not trivial to satisfy, as a simple example illustrates. The Milky Way's (MW) baryonic mass is roughly $\approx 6 \times 10^{10}\,\mathrm{M}_\odot$ (Rix & Bovy 2013), and its rotation velocity is approximately constant at ≈ 220 km s^{-1} over the whole Galactic disc, out to at least 10 kpc. A halo of similar virial velocity, on the other hand, has a virial radius of ≈ 310 kpc and a virial mass of the order of $M_{200} \sim 3.5 \times 10^{12}\,\mathrm{M}_\odot$, or $\approx 6 \times 10^{11}\,\mathrm{M}_\odot$ in baryons, assuming a cosmic baryon fraction of $f_{\rm bar} = \Omega_{\rm b}/\Omega_{\rm M} = 0.17$. A majority of these baryons can, in principle, cool and collapse into the MW disc (see, e.g. White & Frenk 1991). This example illustrates two important points: (i) only a small fraction of available baryons are assembled today at the centre of the MW halo, and (ii) the radius where disc rotational velocities are measured is much smaller than the virial radius of its surrounding halo, where its virial velocity is measured.

These points are quite important for models that try to account for the observed BTF relation. So few baryons assemble into galaxies that it is unclear how, or whether, their masses should scale with virial mass. Furthermore, the disc encompasses such a small fraction of the halo dark matter, and its kinematics probes the potential so far from the virial boundary that a simple scaling between galaxy rotation speed and virial circular velocity might be justifiably discounted. Finally, it is quite conceivable that the mechanism that so effectively limits the fraction of baryons that settle into a galaxy (mainly feedback from evolving stars and supermassive black holes, in current models) might also exhibit large halo-to-halo variations due to the episodic nature of the star formation activity. This makes the rather tight scatter of the observed TF relation quite difficult to explain (McGaugh 2012).

These difficulties explain why the literature is littered with failed attempts to reproduce the TF relation in a cold dark matter (CDM)-dominated universe. Direct galaxy formation simulations, for example, have, for many years, consistently produced galaxies so massive and compact that their rotation curves were steeply declining and, generally, a poor match to observation (see, e.g. Navarro & Steinmetz 2000; Abadi et al. 2003; Governato et al. 2004; Scannapieco et al. 2012, and references therein). Even semi-analytic models, where galaxy masses and sizes can be adjusted to match observation, have had difficulty reproducing the TF relation (see, e.g. Cole et al. 2000; Cattaneo, Salucci & Papastergis 2014), typically predicting velocities at given mass that are significantly higher than observed unless adjustments are made to the response of the dark halo (Dutton & van den Bosch 2009).

The situation, however, has now started to change, notably as a result of improved recipes for the subgrid treatment of star formation and its associated feedback in direct simulations. As a result, recent simulations have shown that rotationally supported discs with realistic surface density profiles and relatively flat rotation curves can actually form in CDM haloes when feedback is strong enough to effectively regulate ongoing star formation by limiting excessive gas accretion and removing low-angular momentum gas (see, e.g. Guedes et al. 2011; Brook et al. 2012; McCarthy et al. 2012; Aumer et al. 2013; Marinacci, Pakmor & Springel 2014; Christensen et al. 2016).

These results are encouraging but the number of individual systems simulated so far is small, and it is unclear whether the same codes would produce a realistic galaxy stellar mass function or reproduce the scatter of the TF relation when applied to a cosmologically significant volume. The role of the dark halo response to the assembly of the galaxy has remained particularly contentious, with some authors arguing that substantial modification to the innermost structure of the dark halo, in the form of a constant-density core or cusp expansion, is needed to explain the disc galaxy scaling relations (Dutton & van den Bosch 2009; Chan et al. 2015), while other authors find no compelling need for such adjustment (see, e.g. Vogelsberger et al. 2014; Lacey et al. 2016; Schaller et al. 2015a).

The recent completion of ambitious simulation programmes such as the EAGLE project (Crain et al. 2015; Schaye et al. 2015), that follow the formation of thousands of galaxies in cosmological boxes ≈ 100 Mpc on a side, allow us for a reassessment of the situation. The subgrid physics modules of the EAGLE code have been calibrated to match the observed galaxy stellar mass function and the sizes of galaxies at $z = 0$, but no attempt has been made to match the BTF relation, that is therefore a true corollary of the model. The same is true of other relations, such as colour bi-modality, morphological diversity, or the stellar-mass TF relation of bright galaxies that are successfully reproduced in the model (Schaye et al. 2015; Trayford et al. 2015). Combining EAGLE with multiple realizations of smaller volumes chosen to resemble the surroundings of the Local Group of Galaxies (the APOSTLE project, see, e.g. Sawala et al. 2016; Fattahi et al. 2016), we are able to study the resulting BTF relation over four decades in galaxy mass. In particular, we are able to examine the simulation predictions for some of the faintest dwarfs, where recent data have highlighted potential deviations from a power-law BTF and/or increased scatter in the relation (Geha et al. 2006; Trachternach et al. 2009).

We begin with a brief description of EAGLE and APOSTLE in Section 2 and present our main results in Section 3. We investigate numerical convergence in Section 3.1. The gas/stellar content and size as a function of galaxy mass are presented in Section 3.2 before comparing the simulated BTF relation with observation in Section 3.3. We examine the predicted faint end of the relation in Section 3.4 before concluding with a brief summary of our main conclusions in Section 4.

2 NUMERICAL SIMULATIONS

2.1 The code

The simulations we use here were run using a modified version of the smoothed particle hydrodynamics (SPH) code P-GADGET 3

[1] We define the virial mass, M_{200}, as that enclosed by a sphere of mean density 200 times the critical density of the Universe, $\rho_{\rm crit} = 3H^2/8\pi G$. Virial quantities are defined at that radius, and are identified by a '200' subscript.

(Springel 2005), as developed for the EAGLE simulation project (Crain et al. 2015; Schaller et al. 2015b; Schaye et al. 2015). We refer the reader to the main EAGLE papers for further details, but list here the main code features, for completeness. In brief, the code includes the 'Anarchy' version of SPH (Dalla Vecchia, in preparation, see also appendix A in Schaye et al. 2015) that includes the pressure-entropy variant proposed by Hopkins (2013), metal-dependent radiative cooling/heating (Wiersma, Schaye & Smith 2009), reionization of Hydrogen and Helium (at redshift $z = 11.5$ and 3.5, respectively), star formation with a metallicity-dependent density threshold (Schaye 2004; Dalla Vecchia & Schaye 2008), stellar evolution and metal production (Wiersma et al. 2009), stellar feedback via stochastic thermal energy injection (Dalla Vecchia & Schaye 2012), and the growth of, and feedback from, supermassive black holes (Springel, Di Matteo & Hernquist 2005; Booth & Schaye 2009; Rosas-Guevara et al. 2015). The free parameters of the subgrid treatment of these mechanisms in the EAGLE code have been adjusted so as to provide a good match to the galaxy stellar mass function, the typical sizes of disc galaxies, and the stellar mass–black hole mass relation, all at $z \approx 0$.

2.2 The simulations

We use two sets of simulations for the analysis we present here. One is the highest resolution 100 Mpc-box EAGLE run (Ref-L100N1504). This simulation has a cube side length of 100 comoving Mpc; 1504^3 dark matter particles each of mass 9.7×10^6 M$_\odot$, the same number of gas particles each of initial mass 1.8×10^6 M$_\odot$, and a Plummer-equivalent gravitational softening length of 700 proper pc (switching to comoving for redshifts higher than $z = 2.8$). The cosmology adopted is that of Planck Collaboration I (2014), with $\Omega_{\rm M} = 0.307$, $\Omega_\Lambda = 0.693$, $\Omega_{\rm b} = 0.04825$, $h = 0.6777$ and $\sigma_8 = 0.8288$.

The second set of simulations is the APOSTLE suite of zoom-in simulations that evolve 12 volumes tailored to match the spatial distribution and kinematics of galaxies in the Local Group (Fattahi et al. 2016). Each volume was chosen to contain a pair of haloes with individual virial mass in the range of 5×10^{11}–2.5×10^{12} M$_\odot$. The pairs are separated by a distance comparable to that between the MW and Andromeda (M31) galaxies (800 ± 200 kpc) and approach with radial velocity consistent with that of the MW-M31 pair (0–250 km s^{-1}).

The APOSTLE volumes were selected from the DOVE N-body simulation that evolved a cosmological volume of 100 Mpc on a side in the *Wilkinson Microwave Anisotropy Probe* (*WMAP-7*) cosmology (Komatsu et al. 2011). The APOSTLE runs were performed at three different numerical resolutions; low (AP-L3), medium (AP-L2), and high (AP-L1), differing by successive factors of 12 in particle mass and $12^{1/3}$ in gravitational force resolution. All 12 volumes have been run at medium and low resolutions, but only two high-resolution simulation volumes have been completed. Table 1 summarizes the main parameters of these simulations.

We use the SUBFIND algorithm to identify 'galaxies'; i.e. self-bound structures (Springel et al. 2001; Dolag et al. 2009) in a catalogue of friends-of-friends (FoF) haloes (Davis et al. 1985) built with a linking length of 0.2 times the mean interparticle separation. We retain for analysis only the central galaxy of each FoF halo, and remove from the analysis any system contaminated by lower resolution particles in the APOSTLE runs. Baryonic galaxy masses (stellar plus gas) are computed within a fiducial 'galaxy radius', defined as $r_{\rm gal} = 0.15\, r_{200}$. We have verified that this is a large enough radius to include the great majority of the star-forming cold gas and stars bound to each central galaxy.

Table 1. Numerical parameters of the APOSTLE and EAGLE simulations. APOSTLE simulations are labelled 'AP' followed by the level of resolution: L3, L2 and L1 (low, medium, and high resolution). The last column summarizes the minimum virial mass required for convergence $M_{200}^{\rm conv}$ in each resolution. See Section 3.1.

Label	Average particle mass DM (M$_\odot$)	Gas (M$_\odot$)	Max softening (proper pc)	$M_{200}^{\rm conv}$ (M$_\odot$)
AP-L1	5.0×10^4	1.0×10^4	94	6.0×10^9
AP-L2	5.9×10^5	1.3×10^5	216	3.0×10^{10}
AP-L3	7.3×10^6	1.5×10^6	500	3.0×10^{11}
EAGLE	9.7×10^6	1.8×10^6	700	3.0×10^{11}

3 RESULTS

3.1 Galaxy formation efficiency and numerical convergence

The left-hand panel of Fig. 1 shows the relation between virial mass, M_{200}, and galaxy baryonic mass, $M_{\rm bar}^{\rm all}$, in our simulations, where $M_{\rm bar}^{\rm all}$ is computed by counting all gas and stellar particles within $r_{\rm gal}$. Shaded regions bracket the interquartile range in $M_{\rm bar}^{\rm all}$ as a function of virial mass for each of the simulation sets, as indicated in the legend. Thick solid lines of matching colours indicate the median trend. Individual symbols indicate results for the high-resolution AP-L1 run, since the total number of galaxies in those two completed volumes is small.

The dashed grey lines indicate the location of galaxies whose masses make up 100 per cent (top), 10 per cent (middle), and 1 per cent of all baryons within the virial radius. Fig. 1 shows that the galaxy formation efficiency is low in all haloes (less than $\approx$20 per cent) and that it decreases steadily with decreasing virial mass. Galaxies in the most massive haloes shown have been able to assemble roughly 15–20 per cent of their baryons in the central galaxy, but the fraction drops to about 1 per cent in $\approx 10^{10}$ M$_\odot$ haloes for the case of AP-L1. Such a steep decline is expected in any model that attempts to reconcile the shallow faint end of the galaxy stellar mass function with the steep low-mass end of the halo mass function (see, e.g. the discussion in section 5.2 of Schaye et al. 2015 and in section 4 of McCarthy et al. 2012).

The left-hand panel of Fig. 1 also shows the limitations introduced by numerical resolution. The results for the various simulations agree for well-resolved haloes, but the mean galaxy mass starts to deviate in haloes resolved with small numbers of particles. This is most clearly appreciated when comparing the results of the median $M_{\rm bar}^{\rm all}$ for each APOSTLE simulation set. AP-L3 results, for example, 'peel off' below the trend obtained in higher resolution runs for virial masses less than $\approx 3 \times 10^{11}$ M$_\odot$. Those from AP-L2, in turn, deviate from the AP-L1 trend below 3×10^{10} M$_\odot$. To define convergence for the high-resolution run, we simply adopt a similar factor of 10 between AP-L2 and AP-L1. These limits are shown with thin vertical lines in the left-hand panel of Fig. 1.

The issue of convergence in simulations including baryons is complex, since increasing resolution means that new physical processes enter into play and it is unclear whether a recalibration of the subgrid physics should or should not be performed (see detailed discussion in Schaye et al. 2015). We adopt here the simple approach of selecting objects for which different resolutions give consistent baryonic masses. Noting that the particle mass (gas plus dark matter) is 8.8×10^6 M$_\odot$ and 6.0×10^4 M$_\odot$ for AP-L3 and AP-L1, respectively, a simple rule of thumb is then that, on average, only haloes resolved with at least 50 000 particles give consistent

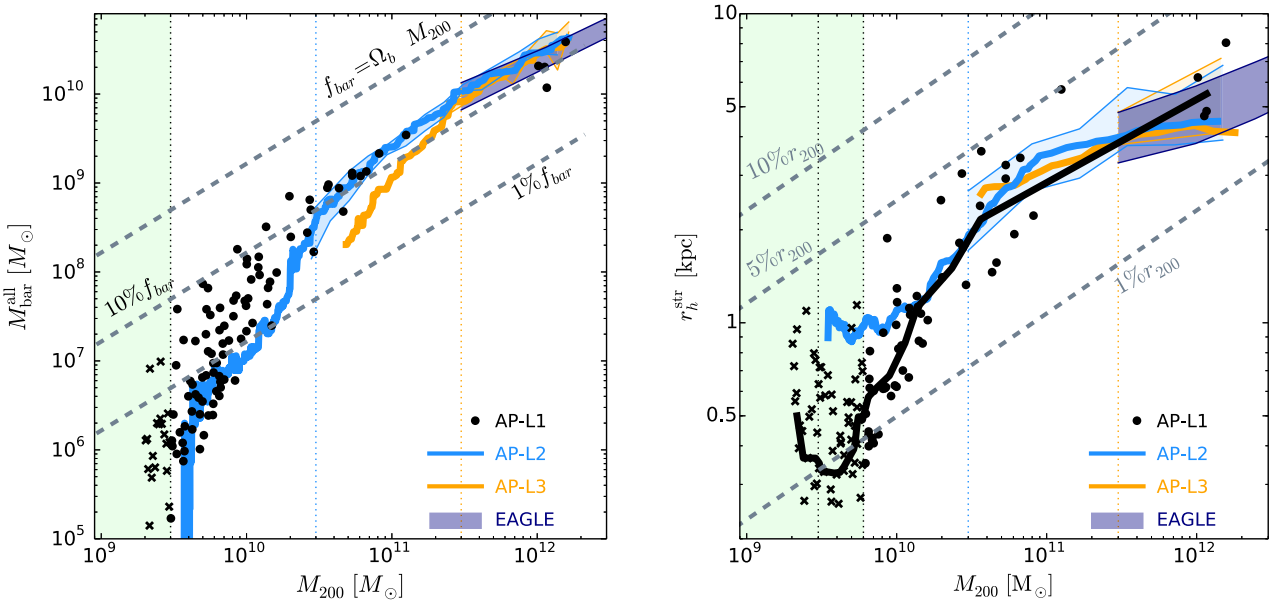

Figure 1. Left: galaxy baryonic mass ($M_{\rm bar}^{\rm all} = M_{\rm gas}^{\rm all} + M_{\rm str}$) versus virial mass ($M_{200}$) in our simulated galaxy sample. Shaded regions indicate the interquartile baryonic mass range at given M_{200} and highlight the virial mass range over which the simulation results are insensitive of resolution. Vertical dotted lines indicate the minimum converged virial mass for each resolution level. Thick lines of matching colour indicate the median trend for each simulation set, as specified in the legend, and extend to virial masses below the minimum needed for convergence. Dashed grey lines indicate various fractions of all baryons within the virial radius. Note the steep decline in 'galaxy formation efficiency' with decreasing virial mass. Dark filled circles indicate the results of individual AP-L1 galaxies. A light green shaded region highlights non-converged systems in our highest resolution runs. Crosses are used to indicate galaxies in haloes considered 'not converged' numerically. Right: stellar half-mass radius, $r_{\rm h}^{\rm str}$, as a function of virial mass for simulated galaxies. Symbols, shading, and colour coding are as in the left-hand panel. Limited resolution sets a minimum size for galaxies in poorly resolved haloes. The same minimum mass needed to ensure convergence in baryonic mass seems enough to ensure convergence in galaxy size, except, perhaps, for AP-L1, for which we adopt a minimum converged virial mass of $6 \times 10^9\,{\rm M}_\odot$. The values adopted for the minimum virial mass are listed in Table 1.

galaxy masses for all runs. We highlight this mass range for each of these runs by shading the interquartile range above the minimum 'converged' mass.

The right-hand panel of Fig. 1 examines convergence in the size of the galaxy (the 3D stellar half-mass radius, $r_{\rm h}^{\rm str}$), as a function of virial mass. This panel shows that galaxy sizes approach a constant value below a certain, resolution-dependent, virial mass. This may be traced to the combined effects of limited resolution and of the choice of a polytropic equation of state for dense, cold gas in the simulations. As discussed by Crain et al. (2015), the equation of state imposes an effective minimum size for the cold gas in a galaxy that explains the constant size of low-mass galaxies seen in the right-hand panel of Fig. 1.

Notably, the same criterion that ensures convergence for galaxy masses appears to ensure convergence in size, as shown by the shaded regions in the right-hand panel that extend down to the same minimum mass as in the left-hand panel. The only exception seems to be AP-L1 where the minimum size is reached at $M_{200} \approx 6 \times 10^9\,{\rm M}_\odot$. We shall hereafter adopt that mass as the minimum halo mass required for convergence for AP-L1. We summarize in Table 1 the minimum virial mass, $M_{200}^{\rm conv}$, of simulated galaxies retained for further analysis.

3.2 Gas content and sizes

Having established numerical convergence criteria for the baryonic mass and size of simulated galaxies – two of the most important ingredients of the BTF relation - we now assess whether 'converged' galaxies compare favourably with observation in terms of their gas, size, and stellar content. Estimates of gas mass in observations are usually derived directly from measurements of neutral hydrogen scaled up by a factor of ≈1.33 or 1.4 in order to take into account the contribution of helium and heavier elements. We note, however, that such procedure can seriously underpredict the total amount of gas, especially for low-mass galaxies, where ionized gas is expected to be an important contributor. Fig. 2 shows the comparison between the total amount of gas within $r_{\rm gal}$ and that in neutral hydrogen (H I) for our simulated galaxies ($M_{\rm H\,I}$ is computed by applying the prescription presented in appendix A.2 of Rahmati et al. 2013). At high masses, the relation is linear with $M_{\rm gas} \approx 2\,M_{\rm H\,I}$ (dotted line), but below $M_{\rm gas} \sim 10^8\,{\rm M}_\odot$, a simple scaling of the neutral hydrogen mass can severely underestimate the total amount of gas in the galaxy due to the increasing importance of ionized gas (see also Gnedin 2012).

We choose therefore to mimic established practice and, in what follows, we shall estimate gas masses in simulated galaxies by $M_{\rm gas}^e = 1.4 M_{\rm H\,I}$ in order to compare with observations. We emphasize, however, that none of our conclusions would change qualitatively if we had used the total amount of gas instead.

Fig. 3 shows the gas versus stellar mass (left-hand panel), as well as the baryonic mass versus(projected) stellar half-mass radius $R_{\rm h}^{\rm str}$ of simulated galaxies, compared with a compilation of observational surveys, as listed in the legends.[2] Note that for consistency

[2] Data taken from Begum et al. (2008), Oh et al. (2011), McGaugh (2012), Adams et al. (2014), Oh et al. (2015) and Bradford et al. (2015). Additionally, we include a subset of the galaxy compilation in Papastergis et al. (2015), including data from the 'Survey of H I in Extremely Low-mass Dwarfs' (Cannon et al. 2011), the 'Local Volume H I Survey' (Trachternach et al. 2009; Kirby et al. 2012), and Leo P (Bernstein-Cooper et al. 2014).

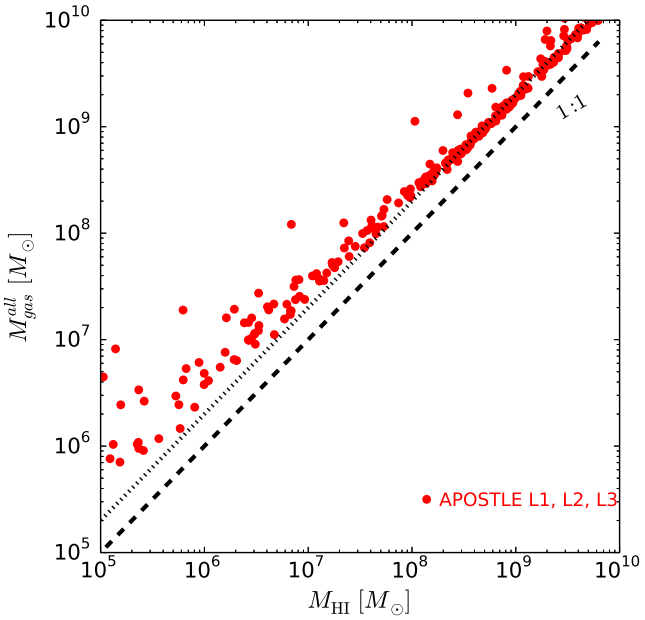

Figure 2. Relation between total gas mass $M_{\rm gas}^{\rm all}$ and the mass in neutral hydrogen $M_{\rm H\,I}$ within $r_{\rm gal}$, computed following the prescription in Rahmati et al. (2013). The dashed line shows the one-to-one relation and the dotted line corresponds to $M_{\rm gas}^{\rm all} = 2\,M_{\rm H\,I}$ that is a good approximation for simulated massive galaxies. Low-mass dwarfs, on the other hand, have a higher fraction of ionized gas and hence their total gas masses may be substantially underestimated by applying to them the same H I scaling factor as for massive systems.

with observations, in the right-hand panel of Fig. 3, sizes in the simulations are computed in 2D (and denoted by capital R to indicate this), by projecting all star particles along a random line-of-sight direction.

This comparison shows that our galaxies reproduce observed trends relatively well, although some differences are worth pointing out. One is the characteristic galaxy mass below which the gas content dominates the baryonic inventory of a galaxy, that happens for $M_{\rm str} \lesssim 5 \times 10^9\,{\rm M}_\odot$ in observed galaxies. In the simulations, although gas is more abundant in low-mass galaxies than in large ones, it rarely dominates the baryonic mass, with an average contribution of about half for galaxies with stellar masses $\lesssim 1 \times 10^9\,{\rm M}_\odot$. On average, $M_{\rm gas}^e/M_{\rm str}$ is a factor of 3 to 4 smaller in simulations than in observations at fixed $M_{\rm bar}^e$. Interestingly, this factor is independent of baryonic mass, suggesting that the star formation efficiency in the simulations may be too high by a similar factor at all masses.

The second point to note is that the stellar component of simulated galaxies at the faint end tends to be slightly larger in size, at fixed $M_{\rm bar}$, than for the observed counterparts (≈50 per cent effect). The reasonable agreement in mass and sizes between observations and simulations implies that estimates of the disc circular velocity from our simulations can reliably be compared with observational measurements. In order to provide a more direct comparison between observed and simulated circular velocities, in what follows, we will only include observed galaxies with spatially resolved rotation curves rather than those estimated from velocity widths.

3.3 The BTF relation

We now proceed to examine the velocity scaling of the baryonic masses. The simulated BTF relation is shown in Fig. 4, where we plot the circular velocity ($V_{\rm c}^2 = GM(r)/r$) estimated at twice the baryonic half-mass radius, $V_{\rm c}(2\,r_{\rm h}^{\rm bar})$, versus $M_{\rm bar}$, the sum of

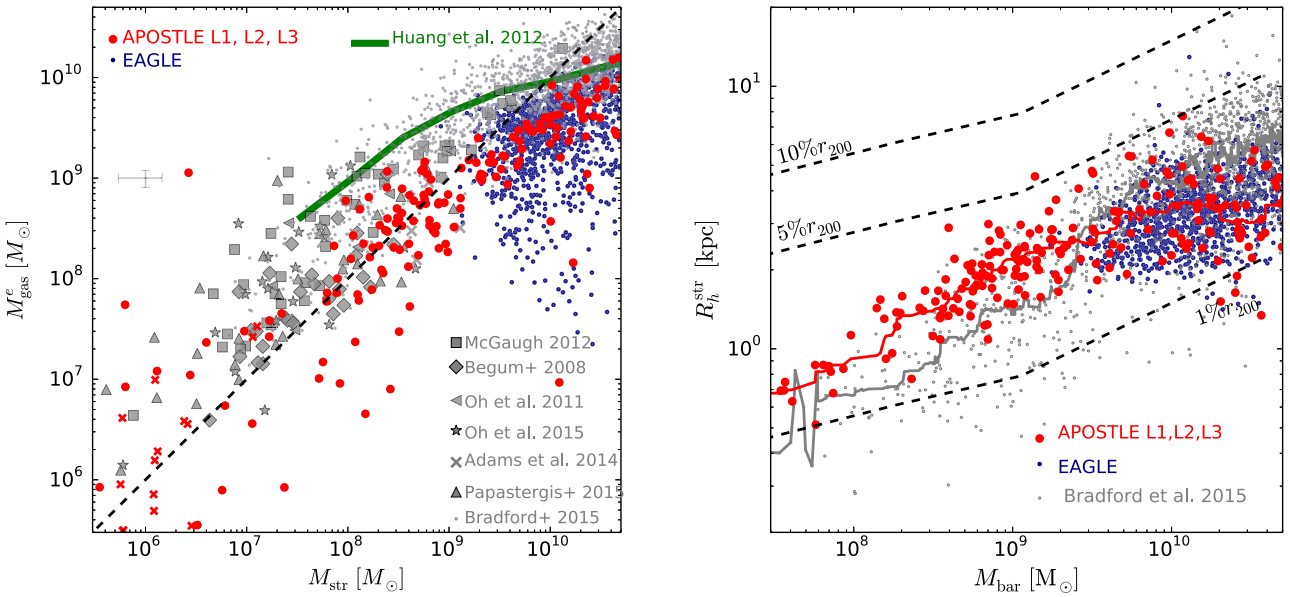

Figure 3. Galaxy properties for our sample of simulated galaxies (red/blue symbols) and for a compilation of observed galaxies taken from the literature (grey symbols). The simulated sample includes all galaxies in haloes above the corresponding minimum converged virial mass (see Table 1). Left: stellar mass versus gas mass relation, where gas masses in observations and simulations are estimated from the H I mass as $M_{\rm gas}^e = 1.4\,M_{\rm H\,I}$. The shape and scatter of the relation agree quite well between the simulations and the observations, although the simulated ratio of the mass in gas to that in stars is three to four times too small at all stellar masses. Green solid line indicates the medium relation from ALFALFA galaxies. Right: baryonic mass ($M_{\rm bar} = M_{\rm str} + M_{\rm gas}^e$) versus stellar half-mass radius ($r_{\rm h}^{\rm str}$) relation. Simulated galaxies are compared with data from Bradford, Geha & Blanton (2015). Simulated galaxies are somewhat smaller than observed for $M_{\rm bar}$ greater than about $2 \times 10^9\,{\rm M}_\odot$, but they are about 50 per cent too big at smaller baryonic mass.

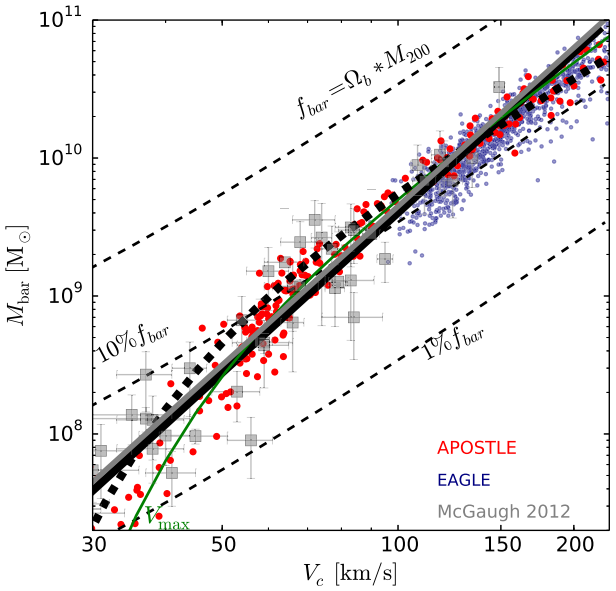

Figure 4. Simulated BTF relation for galaxies with circular velocities in the range $30 < V_c/\ {\rm km\ s^{-1}} < 230$. Symbols and colours are as in Fig. 3. We use the circular velocity at $2\,r_{\rm h}^{\rm bar}$ for simulated galaxies. Grey symbols with error bars show data from the observational compilation of McGaugh (2012) that use the asymptotic 'flat' rotation velocity. Simulations and observations are generally in good agreement. Solid lines indicate the best power-law fits to simulations (black) and observations (grey). The thick black dashed line is a fit to simulated data with steepening slope at the faint end. Parameters of the fit are listed in Table 2. The green thin curve depicts the relation between baryonic mass and the maximum circular velocity of the haloes in our simulations. Note that the slope of the simulated BTF relation is steeper than V^3, as a result of the declining galaxy formation efficiency in low-mass haloes shown in Fig. 1.

the stellar and gas mass (computed as $M_{\rm gas}^e = 1.4 M_{\rm H\,I}$) within $r_{\rm gal}$. Circular velocities measured at $2\,r_{\rm h}^{\rm bar}$ show a roughly one-to-one relation with $V_{\rm c}$ measured at the radius that encloses 90 per cent of the H I mass in each galaxy. It is therefore a good proxy for the velocity measured at the outermost point of the rotation curves in observed galaxies. We focus in Fig. 4 on galaxies with rotation speeds exceeding 30 km s^{-1}, that include most galaxies traditionally used in BTF observational studies, and defer to the next section the analysis of the relation at the very faint end.

A power-law fit to the simulated BTF over this velocity range suggests a relation $M_{\rm bar} = 4.4 \times 10^9 (V_{\rm c}/100\ {\rm km\ s^{-1}})^{3.6}\,{\rm M}_\odot$ (as shown by the black solid line). This may be compared with data for individual galaxies from the compilation of McGaugh (2012) that are shown by the grey squares with error bars, as well as with the power-law fit provided by that reference, $M_{\rm bar} = 4 \times 10^9 (V_{\rm c}/100\ {\rm km\ s^{-1}})^{3.8}\,{\rm M}_\odot$, indicated by the thick grey line.

The differences between the simulated and observed BTF relations are not large, especially considering that we are using all simulated galaxies in the comparison, without selecting for gas content, size, morphology, or rotational support. Galaxies in the observed compilation, on the other hand, are mainly disc systems where the gas component dominates[3] and where the rotation curve

[3] These were purposefully chosen to be gas-dominated in order to minimize uncertainties on their baryonic masses that arise from poorly constrained stellar mass-to-light ratios.

Table 2. Best-fitting parameters to the relation $M_{\rm bar}/{\rm M}_\odot = M_0\,\nu^\alpha \exp(-\nu^\gamma)$, where ν is the velocity in units of 50 km s^{-1}, and can refer to either $V_{\rm max}$ or $V_{\rm out}$ as indicated.

Relation	M_0 (M$_\odot$)	α	γ
$V_{\rm max}$	7.1×10^8	3.08	−2.43
$V_{\rm out}$	1.25×10^9	2.5	−2.00

extends sufficiently far to reach the asymptotic maximum of the rotation curve. Although we do not attempt to match such selection procedures in the simulations, the offset between observed and simulated BTF relations is quite small (at most 20 per cent in velocity for galaxies with baryonic mass of the order of 10^8 M$_\odot$) and would only improve further if we used the maximum asymptotic velocity for the simulated galaxies. The latter is shown by the thin green solid line labelled '$V_{\rm max}$' that shows the fit to the median relation between $M_{\rm bar}$ and $V_{\rm max}$ as given in Table 2 (see also Oman et al. 2015).

The agreement between simulated and observed BTF relations shown in Fig. 4 seems to arise naturally in ΛCDM simulations that broadly reproduce the galaxy mass function and the sizes of galaxies as a function of mass. Its normalization at the luminous end is determined primarily by the need to match the number density of L_* galaxies. This fixes the average galaxy formation efficiency in haloes of virial mass $\approx 2 \times 10^{12}$ M$_\odot$, assigning them a galaxy like the MW (i.e. $M_{\rm bar} \approx 6 \times 10^{10}$ M$_\odot$).

The virial velocity of such haloes, $V_{200} \approx 190$ km s^{-1}, is only slightly below the 220 km s^{-1} derived from the observed BTF relation (grey line in Fig. 4), implying that agreement between simulation and observation follows if the circular velocity traced by the baryons is approximately 15 per cent greater than their virial velocity. This is indeed the case for the whole sample, as shown Fig. 5, where we plot the circular velocity at $2\,r_{\rm h}^{\rm bar}$ as a function of virial velocity for all simulated galaxies. A simple proportionality links, on average, these two measures; i.e. $V_{\rm c}(2\,r_{\rm h}^{\rm bar}) \approx 1.15\,V_{200}$ (see thick dashed line in Fig. 5 showing the median of the points very close to the one-to-one line), exactly what is needed to reconcile the normalization of the simulated and observed BTF relations.

We emphasize that this is not a trivial result, but rather a consequence of the combined effects of (i) the self-similar nature of ΛCDM haloes that regulates the total amount of dark matter enclosed within the luminous region of a galaxy, (ii) the mass and size of the galaxy that specifies the baryonic contribution to the disc rotation velocity; and (iii) the response of the dark halo to the assembly of the galaxy that determines how the halo contracts/expands as baryons collect at its centre. The agreement between observed and simulated BTF shown in Fig. 4 should therefore be considered a major success of this ΛCDM model of galaxy formation.

The simulations also clarify why the simulated BTF relation is steeper than the 'natural' $M \propto V^3$ relation discussed in Section 1. Since rotation velocities are directly proportional to virial velocity (Fig. 5), the steeper slope mainly reflects the fact that galaxy formation efficiency declines gradually but steadily with decreasing halo mass, as required to match the faint end of the galaxy stellar mass function (see left-hand panel of Fig. 1).

The response of the dark halo in the EAGLE/APOSTLE simulations has been discussed in detail in Schaller et al. (2015a,c). We shall not repeat that analysis here, except to point out that for radii as large as $2\,r_{\rm h}^{\rm bar}$, it can be characterized fairly accurately by some

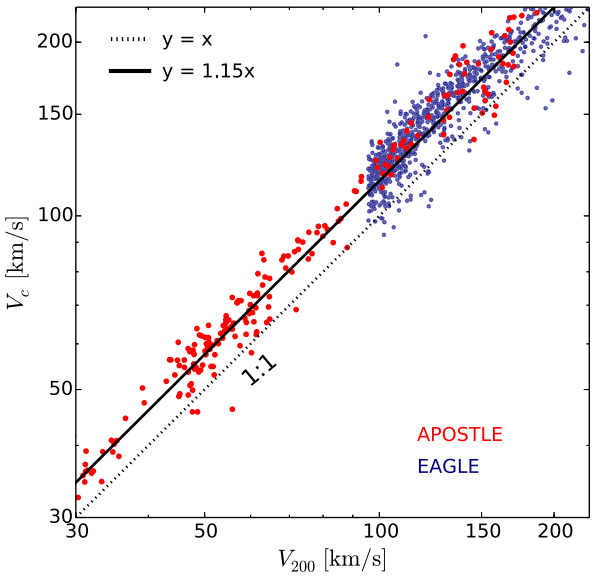

Figure 5. Circular velocity at twice the baryonic half-mass radius, $V_c(2\,r_h^{bar})$, as a function of virial velocity, V_{200}, for simulated galaxies. Symbols are as in Fig. 3. Note that a simple proportionality ($V_c \approx 1.15\,V_{200}$) links these two measures of circular velocity (solid black line). This is not a trivial result, but rather a consequence of the self-similar nature of ΛCDM haloes, of the smooth decline in galaxy size with baryonic mass (Fig. 3), and of the mild response of the halo to galaxy assembly. See the text for more details.

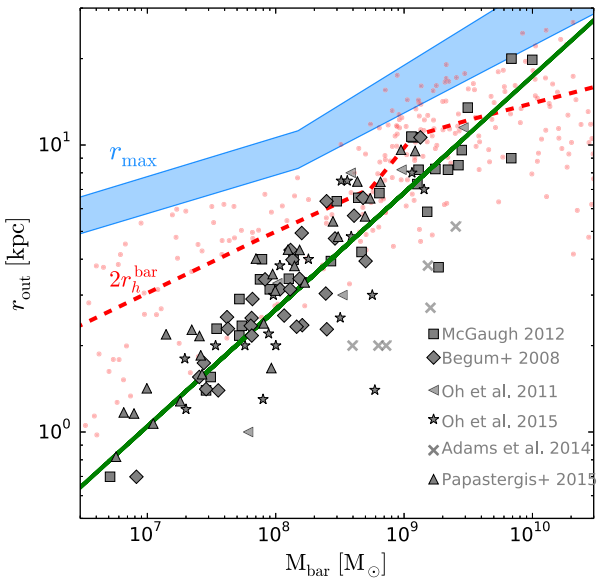

Figure 6. The outermost radius, r_{out}, of the rotation curve of observed galaxies as a function of baryonic mass. The green line shows a power-law fit to the observations $\log(r_{out}/\mathrm{kpc}) = 0.41\,\log(M_{bar}/\mathrm{M}_\odot) - 2.83$. These are typically smaller than $2r_h^{bar}$ (red dots and dashed line for individual galaxies and median, respectively), specially for low-mass galaxies. The blue shaded area brackets, at given M_{bar}, the interquartile range of radii where simulated galaxies reach their peak circular velocity. The limited extent of observed galaxy rotation curves samples only the inner, rising part, of the halo circular velocity curve, especially at the low-mass end, $M_{bar} < 5 \times 10^8\,\mathrm{M}_\odot$. This effect needs to be taken into account when comparing the faint end of the observed and simulated BTF relations (see also Brook & Di Cintio 2015).

mild 'adiabatic' contraction that is only noticeable in the most massive, baryon-dominated galaxies. The galaxy formation efficiency in dwarf galaxy haloes is so low that their inner dark mass profiles are unaffected by the assembly of the galaxies (see also the discussion in Oman et al. 2015).

Finally, we consider the scatter in the simulated BTF relation. A conservative estimate may be derived by considering all simulated galaxies, regardless of morphological type, size, gas fraction, or rotation curve shape. We find an rms scatter of 0.20 dex in mass and 0.05 dex in velocity from the best power-law fit to the data shown in Fig. 4. The scatter is even smaller if, instead of a power law, one considers a relation whose slope steepens slightly towards the faint end.[4] The scatter about this relation is just 0.14 dex in mass and 0.04 dex in velocity. For comparison, the power-law scatter in the observed BTF relation shown in Fig. 4 is 0.2 dex in mass and 0.06 dex in velocity.

The small simulated scatter arises because the efficiency of feedback is tightly coupled to the gravitational potential. Indeed, galaxy masses are tightly correlated with halo mass (as shown in the left-hand panel of Fig. 1) and, consequently, with its potential well depth. This seems to be a natural feature of the numerical scheme for star formation and feedback adopted in the EAGLE/APOSTLE code, where feedback energy is used to heat the gas in star forming regions to very high temperatures, overpressurizing the local environment and 'passively' driving large-scale winds.

We conclude that our simulations have no obvious difficulty accounting for the small scatter in the BTF relation. Actually, the opposite seems true once fainter galaxies are considered, as we discuss next.

[4] These fits are of the form $M_{bar}/\mathrm{M}_\odot = M_0\,\nu^\alpha \exp(-\nu^\gamma)$, where ν is the velocity in units of 50 km s^{-1}. The best-fitting parameters M_0, α, and γ are listed in Table 2.

3.4 The faint end of the BTF relation

The discussion of the previous section has important consequences for the faint end of the BTF relation. If galaxy formation efficiencies drop ever more rapidly with decreasing halo mass (as shown in the left-hand panel of Fig. 1), a sharp steepening of the BTF relation should be expected at the faint end. This is shown explicitly by the thin green line labelled 'V_{max}' in Fig. 4 that shows the median baryonic mass as a function of the maximum asymptotic circular velocity for simulated galaxies. The faint-end steepening is a direct consequence of the increased efficiency of feedback in shallower potential wells, and is therefore a robust prediction of the model.

In order to examine whether this prediction agrees with observation, we need to extend the observational sample to include fainter galaxies than those listed in the compilation of McGaugh (2012). We therefore add to the observed sample galaxies from the THINGS (de Blok et al. 2008; Oh et al. 2011) and LITTLE THINGS (Oh et al. 2015) surveys; those from the compilation of Papastergis et al. (2015), as well as individual galaxies observed by Begum et al. (2008) and Adams et al. (2014).

One issue that arises when enlarging the dwarf galaxy sample in this manner is that in many cases, the rotation curve is still rising at the outermost measured radius and therefore the reported velocity may fall short of the maximum asymptotic value of the system. One way of appreciating this is shown in Fig. 6, where we plot the outermost radius of the rotation curve, r_{out}, versus baryonic mass for all the galaxies in the references listed above. Clearly, the observed radial extent of the rotation curve correlates strongly with baryonic mass: the lower the galaxy mass, the smaller the galaxy, and the shorter its rotation curve. This trend is in sharp contrast with the radius, r_{max}, at which the maximum circular velocity is reached in

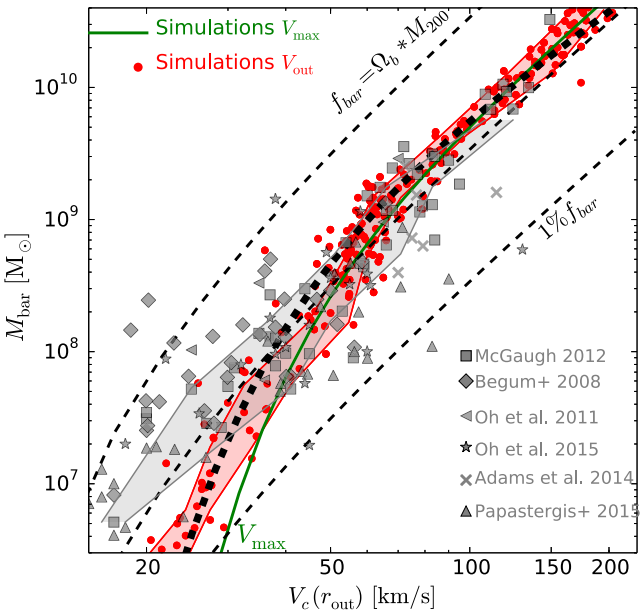

Figure 7. Comparison between predicted and observed baryonic Tully–Fisher relations, extended to include fainter galaxies than in Fig. 4. Grey symbols indicate the observed compilation, from references listed in the legend. Velocities are now defined at r_{out}, the outermost point of the observed rotation curve given in Fig. 6 (or its maximum value, when the two do not coincide). Median values of maximum velocity at given baryonic mass for simulated galaxies are indicated by the thick solid line labelled 'V_{max}'. Small dots indicate the predicted velocities of simulated galaxies measured at the r_{out} based on the best power-law fit to the observed sample (see green line in Fig. 6). The shaded areas correspond to the interquartile velocity range at a given fixed baryonic mass for the simulated (red) and observed (grey) samples. As expected from Fig. 6, $V_c(r_{out})$ underestimates the maximum velocity in low-mass galaxies by a factor of ≈1.5. Note as well that the simulated BTF shows a clear steepening in mass at the faint end that is less pronounced in the observed BTF. The observed BTF also has substantially larger scatter at the faint end, with a number of clear outliers with no counterparts in the simulated sample (see the text for more details).

simulated galaxies. r_{max} flattens out at small masses as a result of the steepening of the M_{bar}–M_{200} relation. Broadly speaking, all dwarfs in Fig. 6 with baryonic masses below $\sim 10^8$ M$_\odot$ inhabit haloes of similar virial mass that results in the very weak dependence of r_{max} with M_{bar} shown in this figure.

Because r_{out} is in many cases much smaller than r_{max} or $2r_h^{bar}$, especially at the low-mass end, it is important that velocities are estimated at similar radii when comparing with observations. We attempt to do this by choosing a value of r_{out} for each simulated galaxy based on its baryonic mass M_{bar} and by randomly sampling the M_{bar}–r_{out} relation shown in Fig. 6. (In practice, we use the power-law fit shown by the solid green line and a Gaussian scatter in radius of 0.15 dex.) This procedure ensures that circular velocities are measured for our simulated galaxies at the same radii, on average, as for observed galaxies of the same baryonic mass. Note that for the small masses of most interest in this paper, both simulated and observed systems are usually dominated by dark matter, so that that the actual distribution of baryons has little effect.

The result of this exercise is shown in Fig. 7, where red solid circles show the predicted V_{out} for simulated galaxies and the shaded areas bracket the interquartile velocity distribution obtained (at fixed M_{bar}). The comparison illustrates a couple of interesting points. One is that, as expected, the rotation velocities at the faint end underestimate the maximum circular velocities by, at times, a fairly large factor. This has the effect of largely rectifying the BTF steepening predicted when using V_{max}, so that the relation at the faint end appears to follow a power-law scaling similar to that of the more luminous systems (see Brook & Di Cintio 2015; Di Cintio & Lelli 2016, for a similar analysis and conclusion). The sharp steepening of the BTF at the faint end may thus be somewhat 'hidden' by the fact that the sizes of galaxies scale strongly with baryonic mass, leading to a systematically larger underestimation of the maximum circular velocity with decreasing galaxy mass (see Papastergis & Shankar 2016; Brook, Santos-Santos & Stinson 2016).

Fig. 7 also highlights a few differences between the observed and simulated the BTF relation at the faint end: (i) the steepening trend seen in the simulated BTF faint end is more pronounced than observed, despite the rectifying effect caused by the small values of r_{out} discussed above, and (ii) the scatter in velocity at given mass is significantly larger in observations.

The first point suggests that, at the very faint end, observed galaxies inhabit haloes of lower mass (or lower circular velocity, to be more precise) than predicted by the model, a result reminiscent of previous conclusions (Ferrero et al. 2012; Papastergis et al. 2015). A similar issue arises when comparing the predicted and estimated masses of MW satellites, also known as the 'too-big-to-fail' problem (Boylan-Kolchin, Bullock & Kaplinghat 2011). The difference is, however, small: the median velocity predicted for galaxies in the range of $5 \times 10^6 < M_{bar}/M_\odot < 3 \times 10^7$ is ≈22 km s^{-1} while the observed value is ≈19 km s^{-1}.

The second point may be best appreciated by considering the dispersion in simulated velocities at given mass that is basically independent of M_{bar} and only of the order of 0.05 dex when measured from the best-fitting function shown by the thick black dashed line. On the other hand, the dispersion in the observed data is much greater: for example, at $M_{bar} \approx 10^8$ M$_\odot$, the velocity rms is 0.13 dex, with some obvious outliers in the observed sample for which there are no simulated counterparts.

The observed outliers in Fig. 7 present a more worrying puzzle. The ones to the right of the simulated trend can, in principle, be explained as baryon-dominated galaxies where the central concentration of baryonic matter leads to rotation velocities that exceed the asymptotic maximum of the halo (i.e. 'declining' rotation curves). The ones on the left, on the other hand, are more difficult to explain. These are galaxies that are extremely massive in baryons for their rotation speed or, alternatively, that rotate much more slowly than is typical for their mass.

Because galaxy formation efficiencies are, almost without exception, very low in simulated dwarf galaxies, the observed baryonic mass of a galaxy places a strong lower limit on the virial mass of the halo it inhabits. The mass of the halo then constrains the total amount of dark matter within r_{out}, placing a strong lower limit on the circular velocity there. The outliers on the left of the simulated trend shown in Fig. 7 are therefore either systems with uncharacteristically high galaxy formation efficiency, or else systems with unusually low dark matter content within r_{out} for their virial mass.

If these galaxies are rotationally supported (such that their measured rotation speed is equal to their circular velocity $V_c(r)^2 = GM(r)/r$), the latter option implies that some dark matter is 'missing' from the inner regions of the halo, leading to a circular velocity at r_{out} that substantially underestimate the true maximum circular velocity of the system. It would be tempting to ascribe this result to the presence of 'cores' in the dark halo but we note that this would imply cores larger than the galaxy itself. Furthermore, in that case, all such outliers should have rising rotation curves that extend out to at least r_{out}. That is indeed the case for the one

simulated point close to the 100 per cent efficiency line (top dashed curve in Fig. 7). In that case, a rotation velocity of $\sim$34.5 km s^{-1} is measured at $r_{\rm out} = 1.5$ kpc, whereas the asymptotic maximum velocity of 62 km s^{-1} is not reached until $r_{\rm max} \sim 18$ kpc. On the other hand, as discussed by Oman et al. (2016), the rotation curves of the observed outliers are typically not rising at their outermost radius.

Inclination errors could also potentially bring some of the outliers back to the main relation. This would, however, require inclination corrections of the order of 15°–30°, well above the estimated uncertainties in current observations (see the detailed discussion in Oman et al. 2016). If more accurate measurements of inclination angles confirm the current estimates, these outliers are truly systems without explanation in our ΛCDM-based model of galaxy formation.

4 SUMMARY AND CONCLUSIONS

We use the APOSTLE/EAGLE suite of cosmological hydrodynamical simulations to examine the scaling between baryonic mass and rotation velocity (the 'BTF' relation) of galaxies formed in a ΛCDM universe. Our main conclusions may be summarized as follows.

We find that the observed BTF relation is reproduced, without further tuning, by galaxy formation simulations that reproduce the galaxy stellar mass function and have galaxy sizes comparable to observed values. In that case: (i) the BTF normalization is largely determined by matching the abundance of L_* galaxies, (ii) the slope is largely dictated by the steady decline in galaxy formation efficiency with decreasing virial mass, and (iii) galaxy rotation velocities are, on average, directly proportional to the halo virial velocities ($V_c \approx 1.15\,V_{200}$). The scatter in the simulated BTF relation is smaller than observed, despite the strong feedback-driven winds that regulate gas accretion and star formation in the simulations.

The agreement between observed and simulated BTF relations above $V_{\rm c} \sim 40$ km s^{-1} does not require, in our simulations, any special adjustment of the inner dark matter density profile (such as the creation of a constant-density 'core' or a substantial expansion of the central cusp) except for a mild contraction of the halo in baryon-dominated systems.

At the very faint end (i.e. rotation velocities $\lesssim$40 km s^{-1}), the simulated BTF relation steepens considerably as a result of the sharp drop in galaxy formation efficiencies in low-mass haloes that is required to match the shallow faint-end of the galaxy stellar mass function. This implies that most faint dwarfs (i.e. $M_{\rm bar} \lesssim 10^9\,{\rm M}_\odot$) should inhabit haloes of very similar virial mass and, consequently, similar maximum circular velocities.

The observed steepening of the BTF relation at the faint end is less pronounced, and is accompanied by larger scatter than expected from the simulations. This disagreement may be reduced by accounting for the fact that low-mass galaxies are physically small: their rotation curves probe only the rising part of the halo circular velocity profile, leading to systematic underestimation of the asymptotic maximum circular velocity.

More difficult to reconcile with simulations is the large scatter at the faint end of the observed BTF relation. The presence of fairly massive galaxies with unexpectedly small rotation velocities is particularly difficult to explain. This is because, given the small galaxy formation efficiency of low-mass haloes inherent to our model, the baryonic mass of a galaxy places a strong lower limit on the halo mass it inhabits, implying much higher velocities than observed. Unless the interpretation of the observational data is in substantial error (perhaps due to severe underestimation of galaxy inclinations), these outliers seem to be either 'missing dark matter' from the inner regions of their haloes, or to have experienced extraordinarily efficient galaxy formation (Oman et al. 2016). Neither possibility is accounted for in our model, and therefore such systems have no counterparts in our simulations.

ACKNOWLEDGEMENTS

We thank the referee for a constructive report that helped improved the first version of this paper. The authors wish to thank S.-H. Oh, E. de Blok, J. Adams, M. Papastergis and J. Bradford for making data available in electronic form. JFN acknowledges a Leverhulme Trust Visiting Professorship hosted at the ICC by CSF. This work was supported by the Science and Technology Facilities Council (grant number ST/F001166/1). RAC is a Royal Society University Research Fellow. CSF acknowledges ERC Advanced Grant 267291 'COSMIWAY' and JFN a Leverhulme Visiting Professor grant held at the Institute for Computational Cosmology, Durham University. This work used the DiRAC Data Centric system at Durham University, operated by the Institute for Computational Cosmology on behalf of the STFC DiRAC HPC Facility (www.dirac.ac.uk). This equipment was funded by BIS National E-infrastructure capital grant ST/K00042X/1, STFC capital grant ST/H008519/1, and STFC DiRAC Operations grant ST/K003267/1 and Durham University. DiRAC is part of the National E-Infrastructure. The research was supported in part by the European Research Council under the European Union Seventh Framework Programme (FP7/2007-2013)/ERC Grant agreement 278594-GasAroundGalaxies.

REFERENCES

Abadi M. G., Navarro J. F., Steinmetz M., Eke V. R., 2003, ApJ, 591, 499
Adams J. J. et al., 2014, ApJ, 789, 63
Aumer M., White S. D. M., Naab T., Scannapieco C., 2013, MNRAS, 434, 3142
Begum A., Chengalur J. N., Karachentsev I. D., Sharina M. E., 2008, MNRAS, 386, 138
Bell E. F., de Jong R. S., 2001, ApJ, 550, 212
Bernstein-Cooper E. Z. et al., 2014, AJ, 148, 35
Booth C. M., Schaye J., 2009, MNRAS, 398, 53
Boylan-Kolchin M., Bullock J. S., Kaplinghat M., 2011, MNRAS, 415, L40
Bradford J. D., Geha M. C., Blanton M. R., 2015, ApJ, 809, 146
Brook C. B., Di Cintio A., 2015, MNRAS, 453, 2133
Brook C. B., Stinson G., Gibson B. K., Wadsley J., Quinn T., 2012, MNRAS, 424, 1275
Brook C. B., Santos-Santos I., Stinson G., 2016, MNRAS, 459, 638
Cannon J. M. et al., 2011, ApJ, 739, L22
Cattaneo A., Salucci P., Papastergis E., 2014, ApJ, 783, 66
Chan T. K., Kereš D., Oñorbe J., Hopkins P. F., Muratov A. L., Faucher-Giguère C.-A., Quataert E., 2015, MNRAS, 454, 2981
Christensen C. R., Davé R., Governato F., Pontzen A., Brooks A., Munshi F., Quinn T., Wadsley J., 2016, ApJ, 824, 57
Cole S., Lacey C. G., Baugh C. M., Frenk C. S., 2000, MNRAS, 319, 168
Crain R. A. et al., 2015, MNRAS, 450, 1937
Dalla Vecchia C., Schaye J., 2008, MNRAS, 387, 1431
Dalla Vecchia C., Schaye J., 2012, MNRAS, 426, 140
Davis M., Efstathiou G., Frenk C. S., White S. D. M., 1985, ApJ, 292, 371
de Blok W. J. G., Walter F., Brinks E., Trachternach C., Oh S.-H., Kennicutt R. C., Jr2008, AJ, 136, 2648
Di Cintio A., Lelli F., 2016, MNRAS, 456, L127
Dolag K., Borgani S., Murante G., Springel V., 2009, MNRAS, 399, 497
Dutton A. A., van den Bosch F. C., 2009, MNRAS, 396, 141
Fattahi A. et al., 2016, MNRAS, 457, 844
Ferrero I., Abadi M. G., Navarro J. F., Sales L. V., Gurovich S., 2012, MNRAS, 425, 2817

Geha M., Blanton M. R., Masjedi M., West A. A., 2006, ApJ, 653, 240
Gnedin N. Y., 2012, ApJ, 754, 113
Governato F. et al., 2004, ApJ, 607, 688
Guedes J., Callegari S., Madau P., Mayer L., 2011, ApJ, 742, 76
Hopkins P. F., 2013, MNRAS, 428, 2840
Kirby E. M., Koribalski B., Jerjen H., López-Sánchez Á., 2012, MNRAS, 420, 2924
Komatsu E. et al., 2011, ApJS, 192, 18
Lacey C. G. et al., 2016, MNRAS, 462, 3854
Lelli F., McGaugh S. S., Schombert J. M., 2016, ApJ, 816, L14
McCarthy I. G., Schaye J., Font A. S., Theuns T., Frenk C. S., Crain R. A., Dalla Vecchia C., 2012, MNRAS, 427, 379
McGaugh S. S., 2012, AJ, 143, 40
McGaugh S. S., Schombert J. M., Bothun G. D., de Blok W. J. G., 2000, ApJ, 533, L99
Marinacci F., Pakmor R., Springel V., 2014, MNRAS, 437, 1750
Mo H. J., Mao S., White S. D. M., 1998, MNRAS, 295, 319
Navarro J. F., Steinmetz M., 2000, ApJ, 528, 607
Oh S.-H., de Blok W. J. G., Brinks E., Walter F., Kennicutt R. C., Jr, 2011, AJ, 141, 193
Oh S.-H. et al., 2015, AJ, 149, 180
Oman K. A. et al., 2015, MNRAS, 452, 3650
Oman K. A., Navarro J. F., Sales L. V., Fattahi A., Frenk C. S., Sawala T., Schaller M., White S. D. M., 2016, MNRAS, 460, 3610
Papastergis E., Shankar F., 2016, A&A, 591, A58
Papastergis E., Giovanelli R., Haynes M. P., Shankar F., 2015, A&A, 574, A113
Pizagno J. et al., 2005, ApJ, 633, 844
Planck Collaboration I, 2014, A&A, 571, A1
Rahmati A., Pawlik A. H., Raičevič M., Schaye J., 2013, MNRAS, 430, 2427
Rix H.-W., Bovy J., 2013, A&AR, 21, 61
Rosas-Guevara Y. M. et al., 2015, MNRAS, 454, 1038
Sawala T. et al., 2016, MNRAS, 457, 1931
Scannapieco C. et al., 2012, MNRAS, 423, 1726
Schaller M. et al., 2015a, MNRAS, 451, 1247
Schaller M., Dalla Vecchia C., Schaye J., Bower R. G., Theuns T., Crain R. A., Furlong M., McCarthy I. G., 2015b, MNRAS, 454, 2277
Schaller M. et al., 2015c, MNRAS, 452, 343
Schaye J., 2004, ApJ, 609, 667
Schaye J. et al., 2015, MNRAS, 446, 521
Springel V., 2005, MNRAS, 364, 1105
Springel V., White S. D. M., Tormen G., Kauffmann G., 2001, MNRAS, 328, 726
Springel V., Di Matteo T., Hernquist L., 2005, MNRAS, 361, 776
Stark D. V., McGaugh S. S., Swaters R. A., 2009, AJ, 138, 392
Steinmetz M., Navarro J. F., 1999, ApJ, 513, 555
Torres-Flores S., Epinat B., Amram P., Plana H., Mendes de Oliveira C., 2011, MNRAS, 416, 1936
Trachternach C., de Blok W. J. G., McGaugh S. S., van der Hulst J. M., Dettmar R.-J., 2009, A&A, 505, 577
Trayford J. W. et al., 2015, MNRAS, 452, 2879
Tully R. B., Fisher J. R., 1977, A&A, 54, 661
Verheijen M. A. W., 2001, ApJ, 563, 694
Vogelsberger M., Zavala J., Simpson C., Jenkins A., 2014, MNRAS, 444, 3684
White S. D. M., Frenk C. S., 1991, ApJ, 379, 52
Wiersma R. P. C., Schaye J., Smith B. D., 2009, MNRAS, 393, 99
Wiersma R. P. C., Schaye J., Theuns T., Dalla Vecchia C., Tornatore L., 2009, MNRAS, 399, 574

This paper has been typeset from a TEX/LATEX file prepared by the author.